RSC Advances

ROYAL SOCIETY OF CHEMISTRY

www.rsc.org/advances

Cite this: DOI: 10.1039/c0xx00000x

www.rsc.org/xxxxxx

ARTICLE TYPE

Enhanced photocatalytic behavior and excellent electrochemical performance of hierarchically structured NiO microspheres

Xiong Wang*[a], Huimin Mao[a] and Yuchen Shan[a]

Received (in XXX, XXX) Xth XXXXXXXXX 20XX, Accepted Xth XXXXXXXXX 20XX

DOI: 10.1039/b000000x

Hierarchically structured nickel oxide microspheres were acquired through calcination of the hydroxide precursor at 400 °C for 4 h. The phase and morphology of the products were characterized by X-ray diffraction (XRD), scanning electron microscopy (SEM), and field emission scanning electronic microscopy (FE-SEM). The synthesized products are pure phase with high crystallinity. And the hierarchical structures assembled from the nanoflakes with thickness of 50 nm have a considerably large specific surface area (165.3 $m^2 \cdot g^{-1}$). The adsorption capacity and photocatalytic activity of the hierarchically structured NiO were evaluated using direct fast bordeaux as target pollutant, indicating high decolorization rate. The effect of pH on the decolorization rate was also analyzed. The electrochemical behavior of NiO as anode material for lithium ion batteries was investigated. The excellent photocatalytic and electrochemical performances of NiO microspheres can be attributed to the unique hierarchical structures.

Introduction

Nickel oxide, as a new type of functional material, has a broad application prospect in the fields of photocatalysts,[1] ceramics,[2] batteries,[3-5] smart windows,[6] and etc. As known, many unique behaviours of NiO strongly rely on its special size and novel morphology. Although many researchers have made a lot of breakthroughs in preparation of nickel oxide with special morphologies, such as nanoplates,[7, 8] nanofibres,[9] hollow microspheres,[10] and self-assembly structures,[11] the fact can't be ignored that toxic raw materials, expensive metal alkoxides and surfactants have been largely involved in these synthesis processes. Therefore, preparing nano/micro-scaled NiO through an environmentally friendly strategy and exploring the exceptional properties have been attracting widespread scientific and technological interest.

Recently, photocatalytic oxidation technology has revealed wide application prospects for the treatment of organic wastewater and has become the main focus of advanced oxidation processes.[12] Compared with traditional water treatment technologies, photocatalytic oxidation technology has the advantages of high efficiency, mild conditions, and completely degradation without secondary pollution. Nano/micro-sized nickel oxide, an important *p*-type semiconductor with larger specific surface area and wide band gap,[13] can be used to decolorize textile wastewater which is hard to deal with for traditional methods.

Furthermore, it has demonstrated that nanoscaled transition metal oxides (TMOs) can be used as high capacity anode materials via a conversion reaction mechanism.[14] Nanostructured TMOs, such as Co_3O_4,[15, 16] MnO_2,[17] Fe_2O_3,[18, 19] Fe_3O_4,[20, 21] have been intensively studied as anode materials for lithium ion batteries (LIBs) aimed at achieving higher specific capacities than graphite. Among them, NiO has attracted considerable attention due to its high capacity, low cost and environmental benignity.

In this paper, nickel oxide microspheres with hierarchical structures were prepared through thermal decomposition of nickel hydroxide precursor, which was obtained from a mixed solvothermal process in the absence of surfactant. The combination of adsorption and photocatalysis of the as-prepared hierarchical structures could effectively promote the decolorization of direct fast bordeaux dye. The electrochemical behaviour of NiO as anode material for lithium ion batteries was also investigated. The excellent electrochemical performance of NiO microspheres can be attributed to the unique hierarchical structure. It is expected to explore a more extensive potential application of TMOs.

Experimental

Synthesis of nickel oxide

All of the reagents were analytical grade and were used as received without further purification. In a typical synthesis, 3 mmol of $Ni(NO_3)_2$ and 1.5 mmol of $CO(NH_2)_2$ were dissolved in 20 mL deionized water, followed by addition of 60 mL absolute ethanol to form a clear green solution. Then, the solution was transferred to a 100 mL Teflon-lined autoclave. After heating in an oven at 120 °C for 10 h, the autoclave was cooled down to room temperature in the air. The resulting pale green slurry was rinsed with deioned water and anhydrous ethanol for three times to remove soluble impurities. Subsequently, it was dried at 100 °C for 6 h. To obtain the final oxide, the as prepared precursor was calcined in muffle furnace at 400 °C for 4 h.

Characterization

The phase composition of samples were analyzed by X-ray diffraction (XRD) using a Bruker D8 advance diffractometer with Cu k_α radiation, employing a scanning rate 1 °/min in the 2θ ranging from 20 to 80°. Scanning electron microscopy (SEM) images were obtained from Carl Zeiss EVO LS-15 microscope at a tube voltage of 100 kV. In order to study the detailed morphology of nickel oxide, the field emission scanning microscope (FESEM, Hitachi SU8000) was operated with an accelerating voltage of 10 kV. The Brunauer–Emmett–Teller (BET) surface area (S_{BET}, $m^2 \cdot g^{-1}$) was calculated using experimental points at a relative pressure of P/P_0 = 0.05–0.25 by measuring the nitrogen adsorption–desorption isotherms at 77 K in an apparatus (GAPP V-Sorb 2800P, China). The optical band gap was estimated from the UV–Vis absorption spectrum recorded on a Shimadzu UV2450 UV–Vis spectrophotometer with an integrating sphere.

Adsorption capability and photocatalytic performance

The adsorption capability and photocatalytic performance of the samples were evaluated by decolorization of target pollutant under the irradiation of mercury lamp. As direct fast bordeaux (abbreviated as DFB) is widely used in dyeing of cotton, viscose, silk fibre, leather and other industrial products, it was selected to act as the target pollutant with an initial concentration of 75 $mg \cdot L^{-1}$.

In the beginning 10 mg NiO powders were added to 30 mL DFB solution in a test tube under vigorous stirring to get well dispersed suspensions. Then the suspensions were moved into the dark and continuously stirred for 30 min in order to achieve the equilibrium of adsorption−desorption. Adsorption ratio can be calculated by the formula as follows: $A = (C_o\text{-}C)/C_o$, where A is adsorption ratio, C_o is the initial concentration, C is the final concentration. Subsequently, the suspensions were exposed to a 500 W high-pressure mercury lamp which was placed 20 cm above the reactor. At given time intervals, 3 mL of the suspensions were sampled and centrifuged. The supernatants were analyzed by monitoring the characteristic absorbance using the UV−Vis spectrophotometer (Shimadzu, UV 2450). Based on the analysis of the strongest characteristic peaks of spectra, the photocatalytic activities of samples were evaluated.

Electrochemical testing

The electrochemical performances of NiO microspheres were investigated as anode material for rechargeable LIBs in CR2032 coin-type cells. The working electrodes were fabricated by pasting slurries of the as-prepared active material (80 wt.%), carbon black (Super P, 10 wt.%) and poly(vinylidene fluoride) (PVDF, 10 wt.%) dissolved in *N*-methyl-2-pyrrolidone (NMP) on Cu foil strips by doctor blade technique. Then the strips were dried at 140 °C for 24 h in an air oven, pressed under 20 MPa pressure and kept at 100 °C for 12 h in a vacuum. Metallic lithium foil was used as the counter electrode. The electrolyte was 1 M $LiPF_6$ in a mixture of ethylene carbonate/diethyl carbonate (EC/DEC, 1/1 by volume); the separator was Celgard 2500. The cells were assembled in a glove box filled with highly pure argon gas. The galvanostatic charge/discharge tests were performed in the voltage range from 0.1 to 3.0 V *vs.* Li/Li^+ at a constant current density of 0.2 C (1 C = 718 $mAh \cdot g^{-1}$). For comparison, the electrochemical performance of NiO nanoparticles with average particle size of 10 nm was also investigated, which was prepared by thermal decomposition of nickel oxalate nanofibers.[22]

Results and discussion

The typical XRD patterns of the as-prepared precursor and the resulting product were depicted in Fig. 1. All the diffraction peaks of Fig. 1a can be indexed as hexagonal β-$Ni(OH)_2$, which are in good agreement with the reported data (JCPDS No. 14-0117). Fig. 1b shows the XRD pattern of the final thermal decomposition product. All the reflections can be indexed to face-centered cubic (*fcc*) NiO phase with lattice constant a = 4.178 Å, which agrees well with the standard data (JCPDS No. 47-1049). No peaks due to $Ni(OH)_2$ were found from the oxide XRD pattern, indicating that $Ni(OH)_2$ was completely decomposed to NiO at 400 °C for 4 h. The broadening of the diffraction peaks indicates the small crystallite size of the oxide product.

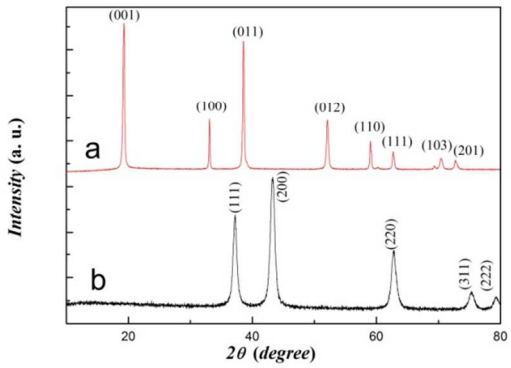

Fig. 1. XRD patterns of (a) the as-prepared precursor and (b) the resulting thermal decomposition product.

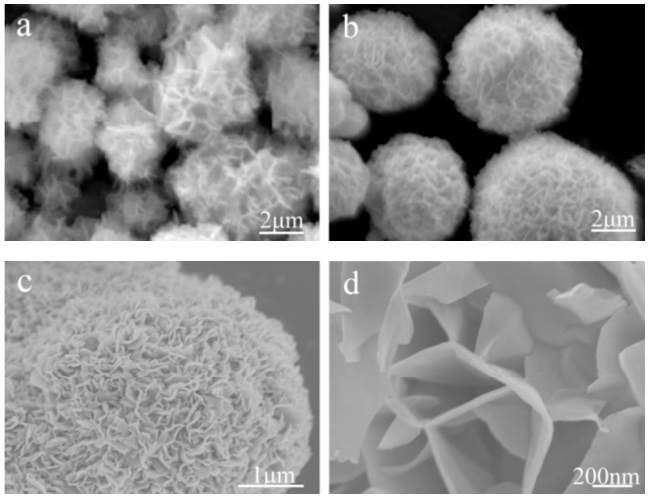

Fig. 2. SEM images of (a) the hydroxide precursor and (b) the oxide product, (c) Low- and (d) high-magnification FESEM images of the oxide product.

Fig. 2 shows the SEM and FESEM images of the precursor and the resulting oxide product. It can be clearly seen that the precursor prepared by the solvothermal method exhibits loosened

sphere-like packing with a diameter range of 4–6 μm, as shown in Fig. 2a. After calcination the oxide product could inherit the morphology of the hydroxide precursor and becomes more compacted with hierarchical structures (Fig. 2b). Fig. 2c and d show the FESEM images of nickel oxide under different magnifications. It can be obviously observed that the hierarchical microspheres with patterned surface are composed of many densely packed and well-defined flake-like structures. These nanoflakes with mean thickness less than 50 nm are interconnected with each other to form hierarchical microspheres. Through the simple two-step method, the hierarchical nanoarchitectures could be achieved without any templates and surfactants. During the solvothermal process, hydroxide ions are gradually released from the hydrolysis of urea, and then consumed by nickel ions leading to the precipitation and succeeding formation of nickel hydroxide nanostructures. The 3-dimensional hierarchical morphology can be maintained after the relatively low-temperature calcination. It could be speculated that these unique structures might have high specific surface area, and consequently they may have high adsorption capability and excellent electrochemical and photocatalytic performances due to easy access of the active species in the reaction process at the interface.

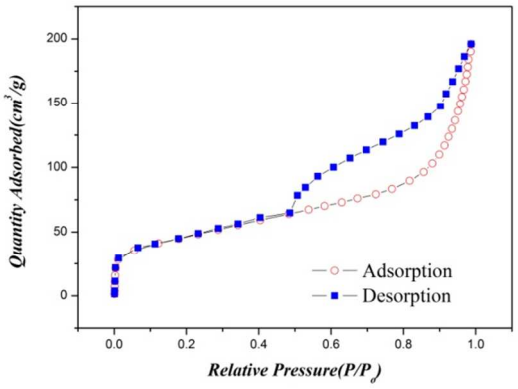

Fig. 3. Nitrogen adsorption-desorption isotherms of hierarchical nickel oxide microspheres.

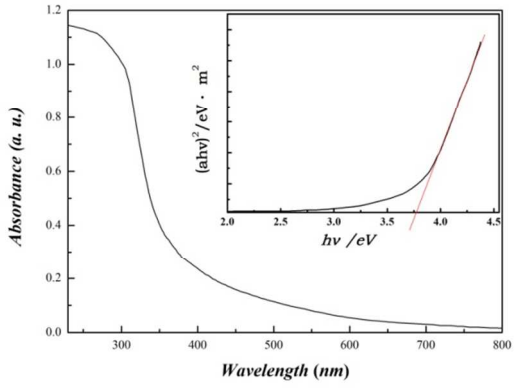

Fig. 4. UV-Vis absorption spectrum of the microspheres and the corresponding $(ahv)^2$–hv curve.

A typical nitrogen adsorption-desorption isotherm of nickel oxide microspheres is shown in Fig. 3. The adsorption isotherm is type II in the classification of Brunauer, Deming, and Teller, whereas the hysteresis loop is of type B in the classification of de Boer.[23] Among the materials showing this type of hysteresis are those in which the macroporous structure is built up of parallel plates, consistent with the morphological observation. The BET surface area of nickel oxide microspheres reaches up to 165.3 m^2/g, benefiting from their hierarchical structures self-assembled from the nanoflakes.

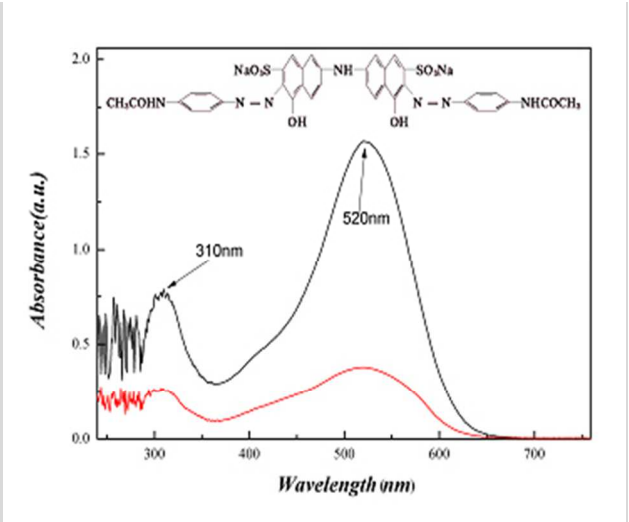

Fig. 5. UV-vis absorption spectra of DFB solution as well as its structural formula.

The optical absorption and energy band feature of a semiconductor are important factors determining its photocatalytic performance. UV-Vis absorption spectrum is usually used to estimate the optical band-gap of nanosized semiconductor. As shown in the absorption spectrum of nickel oxide microspheres in Fig. 4, there is a sharp absorption edge when the wavelength is less than 360 nm which is attributed to the inter-band optical transitions. The band gap is estimated to be 3.76 eV by extrapolation of the equation: $(\alpha hv)^2 = hv\text{-}E_g$, showing in the inset of Fig. 4. The band gap is similar to the value reported before.[22, 24]

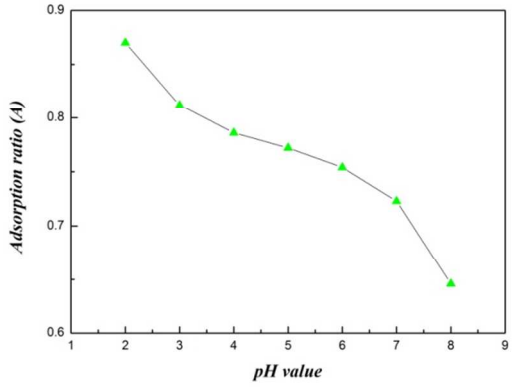

Fig. 6. Dependence of the adsorption ratio (A) on the pH of the solution.

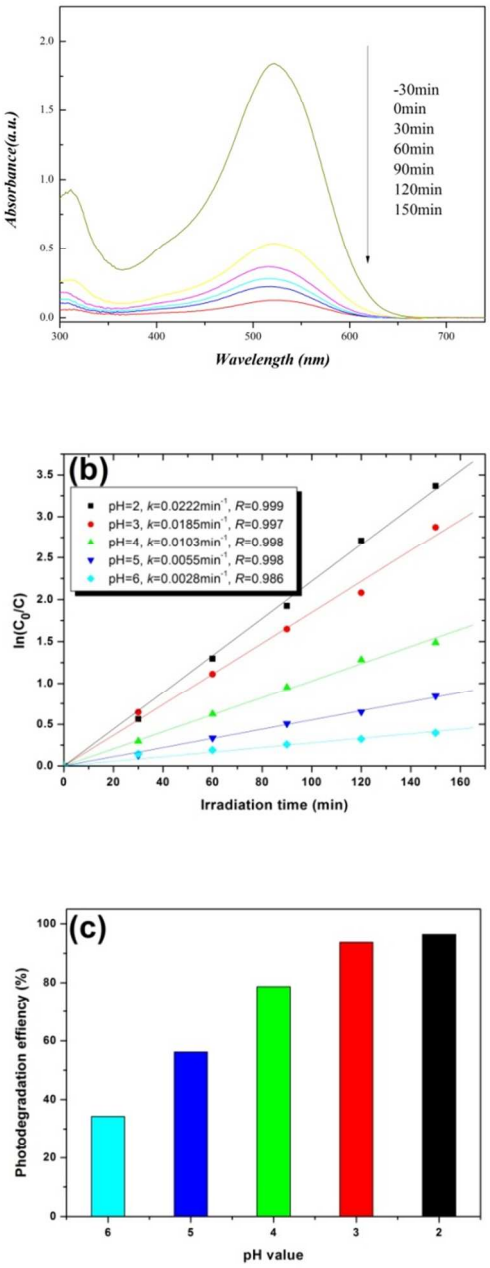

Fig. 7. (a) Absorption spectral changes of DFB solution during the decolorizing process. (b) Photocatalytic reaction kinetics curves and (c) photodegradation efficiency of DFB at different pH values illuminated for 150 min.

To evaluate the adsorption capacity of NiO microspheres, it was determined by absorption of DFB aqueous solution at room temperature. Observed from the UV-Vis absorption spectra of DFB before and after adsorption by the as prepared samples (Fig. 5), two absorption peaks can be obviously seen at the wavelength of 520 nm and 310 nm, which were considered as the characteristic absorption peaks of anthracene, aromatic ring, sulfonic group.[25, 26] The structural formula of DFB was shown in the inset of Fig. 5. It is also found that peak intensity is significantly reduced after adsorption. The adsorption ratio of the sample reaches the highest value of 76.0%, and it is believed to be related to its unique self-assembly hierarchical structure. Besides the influence of specific surface area, this phenomenon also might be closely related to the electrical nature of samples and dye molecules.[27]

In order to further study the effect of the pH on the adsorption activity, the adsorption ratio of the product was tested (as shown in Fig. 6). It can be seen that the adsorption ratio increased significantly with decreasing pH values in the allowable range. As we know, the pH of zero point charge for NiO (pH_{zpc}) is between 8 and 9. At low pH range, NiO surface is positively charged and electrostatic interactions between the positive catalyst surface and the DFB anions lead to strong adsorption of the latter on the NiO support, which will benefit to the subsequent photochemical catalysis.[28] It can be predicted that a higher decolorization ratio could be achieved for the resulting hierarchically structured NiO in acidic media.

To determine the photocatalytic activity of the hierarchical structures, the photocatalytic performances of NiO microspheres were investigated by the degradation of DFB aqueous solution. The temporal photodegradation curves of DFB at pH 2 are revealed in Fig. 7(a). The absorption remarkably decreased and no new peaks were detected, indicating the degradation of DFB. The characteristic absorption at wavelength of 520 nm decreased gradually with the irradiation time and nearly 76.7% DFB in the solution was decomposed within 150 min. The total decolorization ratio of DFB aqueous solution reached 96.4 %.

The amphoteric behaviour of semiconductor oxides influences the surface charge of the photocatalysts. An important parameter governing the rate of photocatalytic reaction taking place on semiconductor particle surface is the pH of the dispersion. By curve-fitting according to the Langmuir-Hinshelwood equation,[29] the photocatalytic performances under different pH conditions are given in Fig. 7(b) with the irradiation time as the horizontal axis and $ln(C_o/C)$ as the longitudinal axis. The results show that the reaction can be considered as a pseudo-first-order reaction by the equation of $ln(C_0/C) = kt$, where k is the pseudo-first-order rate constant, C_0 and C are the DFB concentrations in solution at times 0 and t, respectively. Therefore, the photocatalytic activities can be evaluated by the pseudo-first-order rate constant k. Obviously , the acidity of the dye solution dramatically influences the photocatalytic behaviour of NiO microspheres. The photodegradation efficiency markedly increases with decreasing pH values (Fig. 7c). NiO microspheres exhibit much enhanced photocatalytic activity at pH 2 (k = 0.0222 min^{-1}), almost eight times higher than that of the original DFB solution (pH = 6, k = 0.0028 min^{-1}), which could be attributed to the higher adsorption. As mentioned above, the hierarchical nickel oxide has larger adsorption capacity of DFB molecules in acidic environment. The electrostatic interactions between the positive catalyst surface and the DFB anions will cause the formation of a diffuse electric double layer. Therefore the necessary diffusion distance, a key influence factor of catalytic reaction, was shortened,[30] ultimately improving the photocatalytic properties of the catalyst. Many investigators have observed similar trend with TiO_2, ZnO and $BiFeO_3$.[31-33]

Various nanostructured TMOs have been intensively studied as anode materials for lithium ion batteries. In spite of the higher

specific capacities and volumetric energy densities than the commercial graphite, they still suffer from the dramatic capacity fading. It is believed that the unique hierarchical nanostructures assembled from thin nanoflakes with high surface area can enable the oxide electrode with larger contact area between active material and electrolyte, shorter pathways for lithium ions diffusion, as well as interior macroporous space for alleviating structural strain and volume expansion.[34]

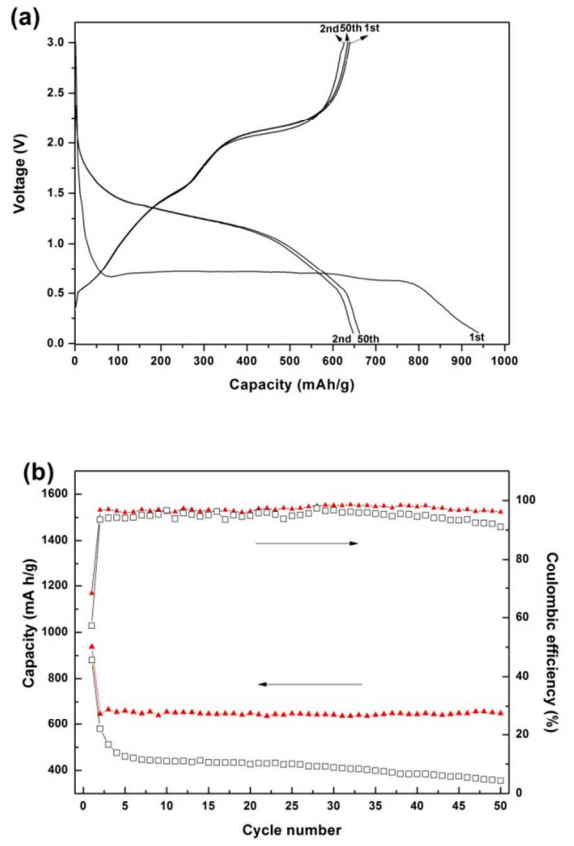

Fig. 8. (a) Galvanostatic discharge/charge curves of the resulting hierarchical NiO electrodes. (b) Cycling performances and the corresponding coulombic efficiencies of the nanoparticulate (hollow squares) and hierarchically structured (solid triangles) NiO for up to 50 cycles at a constant current density of 0.2 C in a voltage window of 0.1–3.0 V *vs.* Li/Li^+.

Herein, the electrochemical measurements for NiO were carried out at room temperature in a voltage range from 3.0 to 0.1 V at a constant current density of 0.2 C up to 50 cycles. Fig. 8(a) shows the galvanostatic discharge/charge curves of the hierarchically structured NiO electrode. The general trend of the charge/discharge curve is consistent with previous reports on NiO anode materials. During the first discharge, the potential rapidly decreases to reach a well-defined plateau (about 0.72 V), corresponding to the reduction of NiO to metallic Ni nanoparticles and the formation of Li_2O and a partially reversible solid electrolyte interphase (SEI) layer. The microspheres exhibit the initial discharge capacity of 938 $mAh \cdot g^{-1}$, much higher than the theoretical value (718 $mAh \cdot g^{-1}$), which is due to the decomposition of electrolyte and the formation of SEI layer in the first discharge. The first charge capacity is about 641 $mAh \cdot g^{-1}$, corresponding to the irreversible capacity loss of 31.7% in the first cycle, which was mainly attributed to the irreversible formation of SEI layer. The same phenomenon was also observed for other TMO anode materials.[35–38] From the second cycle onward, the discharge voltage plateau shifts to 1.5–1.0 V and the reversible specific discharge capacity gradually decreases and ultimately maintains in the range of 647–662 $mAh \cdot g^{-1}$ up to 50 cycles.

The cycling performances of the cells are represented in Fig. 8(b). It can be seen that the hierarchically structured microspheres have higher reversible capacities and much better capacity retention compared with the nanoparticles. The discharge capacity of microspheres after 50 cycles is as high as 650 $mAh \cdot g^{-1}$. In contrast, the nanoparticles exhibit obvious capacity fading. The specific capacity of the nanoparticles decreases continuously and is attenuated to ca. 355 $mAh \cdot g^{-1}$ after 50 cycles. The obvious irreversible capacity fading could be due to the smaller particle size (~10 nm). As we know, during the galvanostatic discharge process, the oxide nanoparticles are reduced into much finer metal nanoparticles. The formed Ni^0 nanoparticles with higher reactivity will promote the electrolyte decomposition and the formation of SEI layer and hinder the charge transfer, leading to the irreversible capacity loss. The corresponding coulombic efficiencies of the nanoparticulate and hierarchically nanostructured NiO for each cycle are revealed in Fig. 8(b). The efficiency of the hierarchical architectures is initially 68.2% and subsequently becomes stabilized and approaches 96% above. In comparison, the coulombic efficiency of the nanoparticles is relatively lower throughout the whole cycles. The efficiency of the 50th cycle for the nanoparticles is only 91%.

Comparatively, the improvement of the reversible capacity and cycleability for the oxide microspheres may be attributed to the unique hierarchical structures. Firstly, the hierarchical structures self-assembled from nanoflakes have a large surface area providing more reaction active sites, and the macroporous structures between the nanoflakes favour the access of the electrolyte. All these will facilitate the intercalation-deintercalation of more lithium ions. Furthermore, the reaction between NiO and lithium ions causes volume changes.[39, 40] Whereas the porous hierarchical structures will relax the tension and buffer against the local volume changes during repeated lithiation/delithiation, which helps to achieve excellent cycleability.

Conclusions

Hierarchically structured nickel oxide has been synthesized through a facile thermal decomposition of nickel hydroxide precursor. The microspherical hierarchical structures were assembled by nanoflakes with thickness of 50 nm, having a specific surface area of 165.3 $m^2 \cdot g^{-1}$. The decrease of absorption peaks of DFB shows that it can remove direct fast bordeaux from wastewater efficiently through adsorption and photodegradation. Based on the analysis of photocatalytic reaction kinetics curves, it is found that the prepared nickel oxide has high-efficiency UV light photocatalytic activity. At lower pH range, higher decolorization ratio could be achieved for the resulting

hierarchically structured NiO due to the higher adsorption capacity. The oxide microspheres as anode material for lithium ion battery exhibit high reversible capacity and excellent cycleability. Large surface area and macroporous structures assembled from thin nanoflakes benefit to the acquisition of high electrochemical capacity and superior capacity retention. The enhancement of electrochemical performance and photocatalytic property for the microspheres may be attributed to their unique hierarchical structures.

Acknowledgements

We gratefully acknowledge the financial supports from the National Natural Science Foundation of China (21001064), the Natural Science Foundation of Jiangsu Province (BK2010487), the Specialized Research Fund for the Doctoral Program of Higher Education of China (20103219120045), and the NUST Research Funding (2011ZDJH27).

Notes and references

[a] *School of Materials Science and Engineering, Nanjing University of Science and Technology, Nanjing 210094, China. Fax: +86-25-84313349; Tel: +86-25-84313349; E-mail: xiongwang@njust.edu.cn*

1 M. Takeuchi, H. Yamashita, M. Matsuoka, M. Anpo, T. Hirao, N. Itoh and N. Iwamoto, *Catal. Lett.*, 2000, **67**, 135-137.
2 J. Wu, C. W. Nan, Y. Lin and Y. Deng, *Phys. Rev. Lett.*, 2002, **89**, 217601.
3 H. Liu, G. X. Wang, J. Liu, S. Z. Qiao and H. J. Ahn, *J. Mater. Chem.*, 2011, 21, 3046.
4 X. Wang, L. Li, Y. G. Zhang, S. Wang, Z. D. Zhang, L. F. Fei and Y Qian, Cryst. Growth Design, 2006, 6, 2163.
5 M. Khairy and S. A. El-Safty, RSC Adv., 2013, 3, 23801.
6 G. A. Niklasson and C. G. Granqvist, J. Mater. Chem., 2007, 17, 127.
7 X. Zhang, W. Shi, J. Zhu, W. Zhao, J. Ma, S. Mhaisalkar, T. L. Maria, Y. H. Yang, H. Zhang, H. H. Hng and Q. Y. Yan, Nano Res., 2010, 3, 643.
8 S. Q., Ci, J. P. Zou, G. S. Zeng, Q. Peng, S. L. Luo and Z. H. Wen, RSC Adv., 2012, 2, 5185.
9 H. Guan, C. Shao, S. Wen, B. Chen, J. Gong, and X. Yang, *Inorg. Chem. Commun.*, 2003, **6**, 1302.
10 X. Song and L. Gao, *J. Phys. Chem. C*, 2008, **112**, 15299.
11 C. Yuan, X. Zhang, L. Su, B. Gao and L. Shen, *J. Mater. Chem.*, 2009, **19**, 5772.
12 D. Chen and A. K. Ray, *Chem. Eng. Sci.*, 2001, **56**, 1561.
13 J. Zaanen, G. A. Sawatzky and J. W. Allen, *Phys. Rev. Lett.*, 1985, **55**, 418.
14 P. Poizot, S. Laruelle, S. Grugeon, L. Dupont and J. M. Tarascon, *Nature*, 2000, **407**, 496.
15 X. W. Lou, D. Deng, J. Y. Lee, J. Feng, L. A. Archer, *Adv. Mater.*, 2008, **20**, 258.
16 X. Wang, X Chen, L Gao, H Zheng, Z. D. Zhang and Y. T. Qian, *J. Phys. Chem. B*, 2004, **108**, 16401.
17 W. Xiao, D. Wang and X. W. Lou, *J. Phys. Chem. C*, 2009, **114**, 1694.
18 X. Wang, L. Gao, H. Zheng, M. Ji, T. Shen and Z. Zhang, *J. Cryst. Growth*, 2004, **269**, 489.
19 B. Wang, J. S. Chen, H. B. Wu, Z. Wang and X. W. Lou, *J. Ame. Chem. Soc.*, 2011, **133**, 17146.
20 W. M. Zhang, X. L. Wu, J. S. Hu, Y. G. Guo and L. J. Wan, *Adv. Funct. Mater.*, 2008, **18**, 3941.
21 B. Wang, H. B. Wu, L Zhang and X. W. Lou, *Angew. Chem. Int. Ed.*, 2013,**52**, 4165.
22 X. Wang, J. Song, L. Gao, J. Jin, H. Zheng and Z. Zhang, *Nanotechno.*, 2005, **16**, 37.
23 J. M. Thomas and W. J. Thomas, *Introduction to the Principles of Heterogeneous Catalysis*: Academic Press, London, 1967.
24 H. Ohta, M. Hirano, K. Nakahara, H. Maruta, T. Tanabe, M. Kamiya, T. Kamiya and H. Hosono, *Appl. Phys. Lett.*, 2003, **83**, 1029.
25 B. T. Commins, *Analyst*, 1958, **83**, 386.
26 Y. Xie and C. Yuan, *Appl. Catal. B: Environ.*, 2003, **46**, 251.
27 M. Vautier, C. Guillard and J. M. Herrmann, *J. Catal.*, 2001, **201**, 46.
28 S. Sakthivel, B. Neppolian, M.V. Shankar, B. Arabindoo, M. Palanichamy and V. Murugesan, *Sol. Energy Mater. Sol. Cells*, 2003, **77**, 65.
29 X. Wang, F. Gu, L. Li, G. Fang and X. Wang, *Mater. Res. Bull.*, 2013, **48**, 3761.
30 S. Y. Lin, K. McKeigue and C. Maldarelli, *AIChE J.*, 1990, **36**, 1785.
31 S. Naskar, S. A. Pillay and M. Chanda, *J. Photochem. Photobiol. A*, 1998, **113**, 254.
32 A. Sharma, P. Rao, R.P. Mathur and S.C. Ametha, *J. Photochem. Photobiol. A*, 1995, **86**, 197.
33 X. Wang, Y. Lin, X. Ding and J. Jiang, *J. Alloys Compd.*, 2011, **509**, 6585.
34 Z. Y. Wang, L. Zhou and X. W. Lou,Adv. Mater., 2012, **24**, 1903.
35 X. W. Lou, Y. Wang, C. L. Yuan, J. Y. Lee and L. A. Archer, *Adv. Mater.*, 2006, **18**, 2325.
36 X Wang, X Chen, L Gao, H Zheng, M Ji, C Tang, T Shen and Z Zhang, *J. Mater. Chem.*, 2004, **14**, 905.
37 L Gao, X Wang, L Fei, M Ji, H Zheng, H Zhang, T Shen and K Yang, *J. Cryst. Growth*, 2005, **281**, 463.
38 J Song, X Wang, X Ni, H Zheng, Z Zhang, M Ji, T Shen, X Wang, *Mater. Res. Bull.*, 2005, **40**, 1751.
39 H. B. Wu, J. S. Chen, H. H. Hng and X. W. Lou, *Nanoscale*, 2012, **4**, 2526.
40 H. Zhang, X. Yu and P. V. Braun, *Nat. Nanotechnol.*, 2011, **6**, 277.

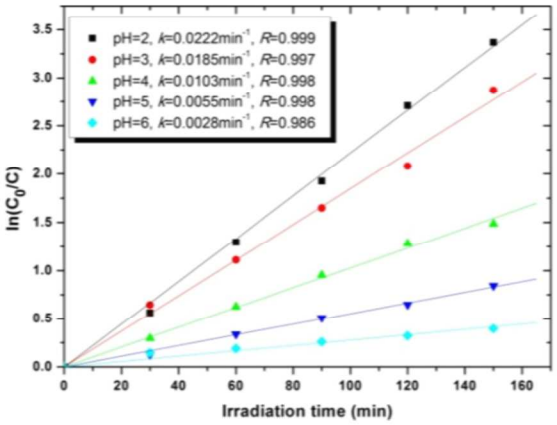

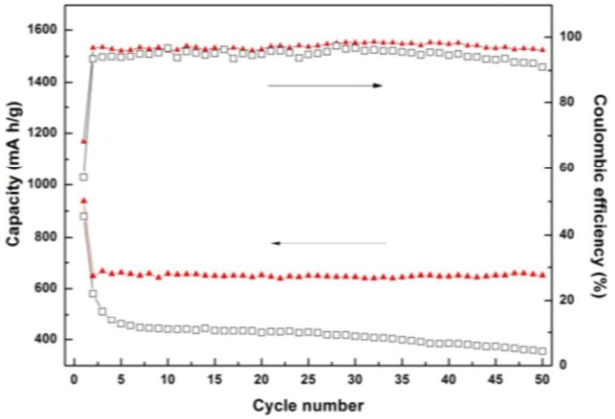

The obtained hierarchically structured nickel oxide exhibits excellent photocatalytic and electrochemical performances.